Testing New Aspects of Deep Inelastic Scattering in *ep* Collision Experiments at HERA

by

N. A. Pavel

Testing New Aspects of Deep Inelastic Scattering
in *ep* Collision Experiments at HERA

Nikolaj A. Pavel

[1] *II. Institute of Experimental Physics, University of Hamburg*

Abstract

With the *ep* collider at HERA the deep inelastic scattering (DIS) process can be studied at much higher values of the $\gamma^* p$ centre-of-mass energy, W. This allows not only to measure the proton structure function F_2 in a new region of the Bjorken scaling variable x and the four momentum transfer Q, but also to test the perturbative QCD effects in the hadronisation more extensively than in fixed target DIS experiments. The measured strong rise of F_2 towards small x at fixed Q^2 is related to the strong increase of the $\gamma^* p$ cross section with W^2, which is in marked contrast to the observed behaviour of the photoproduction cross section. Recent results on these topics from ZEUS and H1 are presented and dicussed. In the DIS event sample a class of events characterised by a large rapidity gap between the observed hadronic final state and the proton direction (LRG events) was found. First results on the cross section and the analysis of the hadron distributions of these species of DIS events are shown. In particular, the question is addressed, how these events can be interpreted and which conclusion concerning the nature of the pomeron can be drawn.

1   Introduction

Deep inelastic lepton nucleon scattering (DIS) experiments have played an important role in exploring the nuclear substructure and testing QCD by measuring inclusive and semi-inclusive distributions [1, 2, 3]. At HERA, which is the world first *ep* collision machine, centre-of-mass energies of 300 GeV can be reached as compared to about 30 GeV in fixed target experiments allowing the study of DIS in a new kinematic regime.

The basic deep inelastic *ep* scattering process is illustrated in Fig.1 and the variables used to describe the process are defined in Table 1. The incoming electron couples to the proton by the exchange of a virtual boson (γ, Z^0 for neutral current (NC) and $W^\pm$ for charged current (CC) reactions). Here I will discuss only NC reactions in the kinematic range, where the γ^*-exchange is dominant. The internal structure of the proton is probed by the photon at a resolution which is proportional to $1/\sqrt{Q^2}$, where Q^2 is the negative square of the four-momentum transfer between the electron and proton. In the quark parton model (QPM) the photon couples to a quark in the proton, which carries the fraction x of the proton's light cone momentum.

Fixed target experiments have been limited to values of $x \gtrsim 10^{-2}$ at $Q^2 \gtrsim 4\,\mathrm{GeV}^2$. At HERA the measurements can be extended to $x \approx 10^{-4}$ at $Q^2 \approx 10\,\mathrm{GeV}^2$. This allows to investigate strongly interacting objects at high densities and values of Q^2, where the strong coupling constant α_s is sufficiently small to

---

[1]invited talk, ICTP '95 Conference, Trieste, May 1995
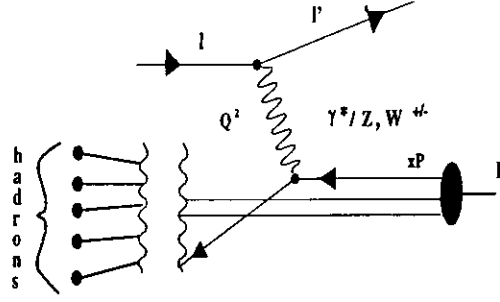
Fig. 1. Schematic diagram of deep inelastic ep scattering.

Variable	Description
$l\ (l')$	Four-momentum of incident (scattered) lepton
P, M_p	Four-momentum of proton and its mass
$Q^2 = -q^2 = -(l - l')^2$	Negative invariant mass squared of exchanged virtual boson
$x = Q^2/(2Pq)$	Bjorken scaling variable
$y = (Pq)/(Pl)$	Inelasticity parameter
$W^2 = (P + q)^2$	square of the $\gamma^* p$ centre-of-mass energy
$\quad = Q^2(1 - x)/x + M_p^2$	invariant mass square of the hadronic final state
P'	four momentum of the outgoing leading proton in LRG events
$x_{pom} = 1 - P'/P$	fraction of the proton momentum transfered to the γ^*
$\beta = x/x_{pom}$	in the pomeron exchange picture: fraction of the pomeron momentum carried by a constituent of the pomeron
$M_X = (x_{pom}P + q)^2$	invariant mass of the hadronic final state observed
$\quad = Q^2(1 - \beta)/\beta$	

Tab. 1. Definition of the variables to describe the kinematics of the inclusive DIS process (upper part) and of the LRG events discussed in section 4 (lower part of the table).

apply perturbative QCD. Furthermore, the vast increase of invariant mass of the hadronic final state, W, significantly enlarges the potential for testing QCD in semi-inclusive DIS processes.

In this report I focus on recent results on DIS from the H1 and ZEUS experiment at HERA, which questioned our present understanding of the DIS process and might call for an refinement or modification of the physics picture, to better describe the process. In the section 2 recent measurements of the proton structure function F_2 and the total photon-proton cross section are discussed, in section 3 selected results from the analysis of the hadronic final state are presented. The section 4 is devoted to the discussion of inclusive and semi-inclusive distributions of DIS events, which are distinguished by a large rapidity gap between the hadronic final state observed and the proton direction (LRG events). In the last section the conclusions are given and some questions are discussed, which have been raised in view of the new experimental results at HERA.

2 Inclusive DIS Cross Section and F_2

The results on the proton structure function F_2 presented here have been determined mainly from the 93 data sample, which represents about a twenty fold increase of integrated luminosity over that used for

the first F_2 measurements [5, 4]. Using data of 1994 with the interaction point shifted w.r.t. the nominal position, it was possible to extend the measurements to lower values of Q^2 (2 GeV^2).

The inclusive DIS cross section can be written in the following form:

$$\frac{d^2\sigma}{dxdQ^2} = \frac{2\pi\alpha^2(1+1-y)^2)}{xQ^4}F_2(x,Q^2)(1-\delta_{FL}+\delta_Z)(1+\delta_r) \tag{1}$$

The term δ_Z represents the contribution from the parity violating structure function F_3 arising from the Z^0 exchange which is for the Q^2 bins shown here negligibly small. However, the correction for the contribution from the cross section of longitudinal polarised photons (δ_{FL}) and the QED radiative correction (δ_r) have to be considered. They are function of x and Q^2 but are, to a good approximation, independent of F_2. The measured cross sections are directly unfolded back to the the virtual photon F_2 using equation 1 using a Monte Carlo event sample, in which the effects of acceptance and migration as well as the correction terms $\delta_{FL,Z,r}$ are considered.

ZEUS/H1/NMC F$_2$
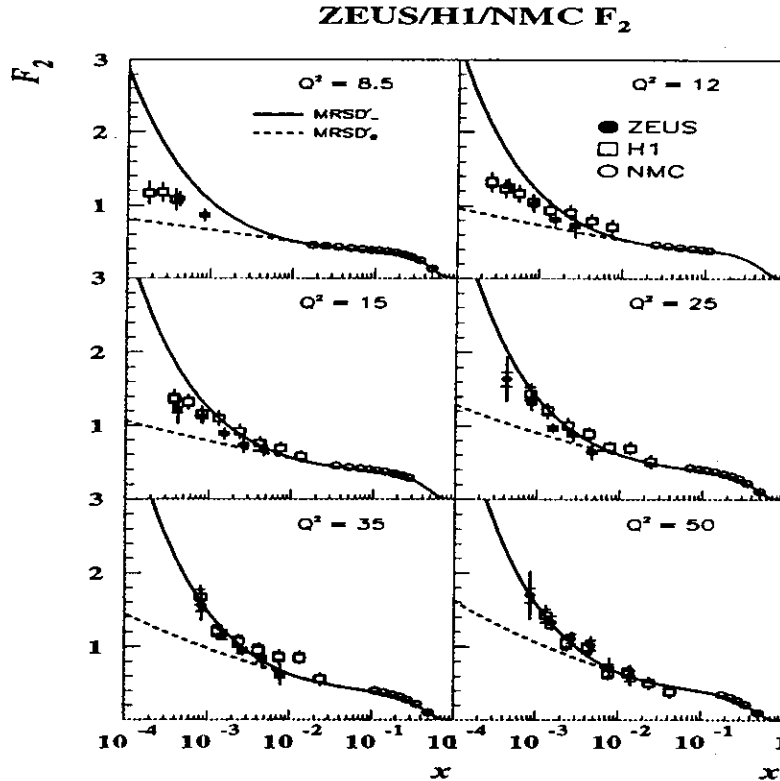
Fig. 2. Proton structure function F_2 as function of x at fixed Q^2 from the HERA ep collision experiments [6, 7]. The results are compared with measurements of a fixed target DIS experiment [8] and with some PDF calculations: $MRSD'_-$ (full line) and $MRSD'_0$ (dashed line).

The values of F_2 from the HERA experiments [6, 7] are shown in Fig. 2 as a function of x in the Q^2 bins together with results from the fixed target experiment NMC [8]. The Figure shows a strong rise of F_2 with decreasing x at fixed Q^2. This behaviour is in striking contrast to to the almost constant behaviour seen in the fixed target experiments at larger values of x. The curves of the $MRSD'_-$ (full line) and the $MRSD'_0$ (dashed line) parameterisation of the parton distribution functions (PDF's) [10] which represent roughly the two extremes of the parameterisations that fit the data at high x. In both

3
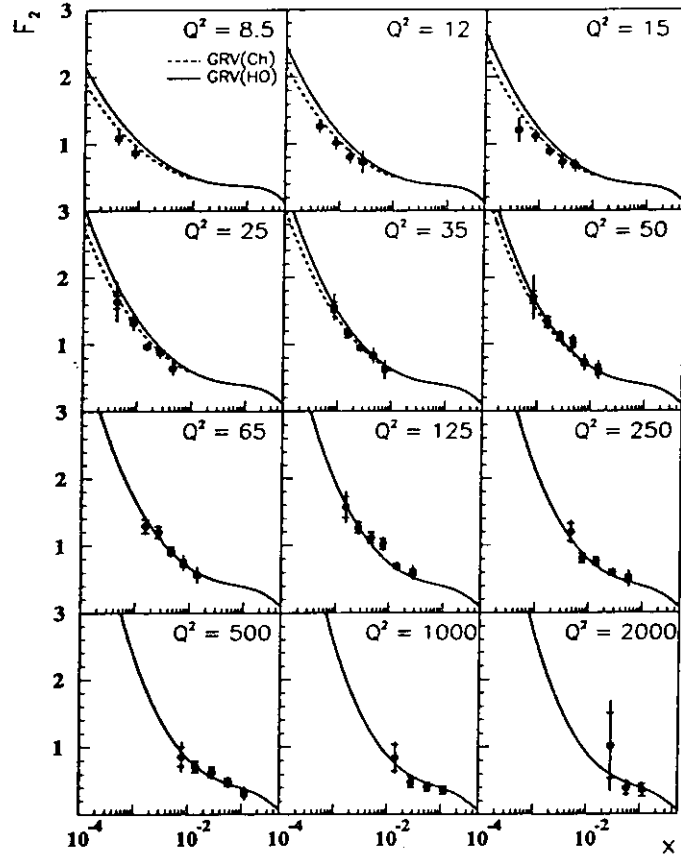
Fig. 3. The measured F_2 values in bins of Q^2 (given in GeV^2) from [6] compared with the GRV(HO) PDF calculation [9] (solid line). For the six lowest Q^2 bins shown, the dashed line displays the results of the GRV(HO) calculation modified for $x < 10^{-2}$ to consider the finite charm quark mass.

calculations the PDF's are evolved from $Q_0^2 = 4$ GeV^2 using the GLAP evolution equations [11]; $MRSD'_-$ starts the evolution with singlular parametrisation for the sea and gluon distributions $xq(x) \to x^{-1/2}$ for $x \to 0$ and with $MRSD'_0$ a PDF which is $xq(x) \to const.$ for $x \to 0$. The data can be parameterised by $F_2 \propto x^{-(0.35+0.16 \lg Q^2)}$, which rules out the latter case. The increase of F_2 is well described by the GRV prediction [9] (see Fig. 3), where the PDF's are evolved from a very low value for $Q_0^2 = 0.3$ GeV^2 starting with valence like quark distributions and a small gluon component. The rise of F_2 is then generated dynamically by gluon radiation and $q\bar{q}$ pair production as described by the GLAP evolution equations. At the present state of the data analysis it is not possible to discriminate already between the BFKL [12] and the GLAP evolution scheme.

The distribtion function of the gluons $xg(x, Q^2)$, which carry about half of the proton momentum, can only be extract indirectly, i.e. exploiting the QCD Compton and boson-gluon-fusion (BGF) process. At small x, $x < 10^{-2}$, the BGF process dominates the scale violation. There have been three methods used

ZEUS 1993
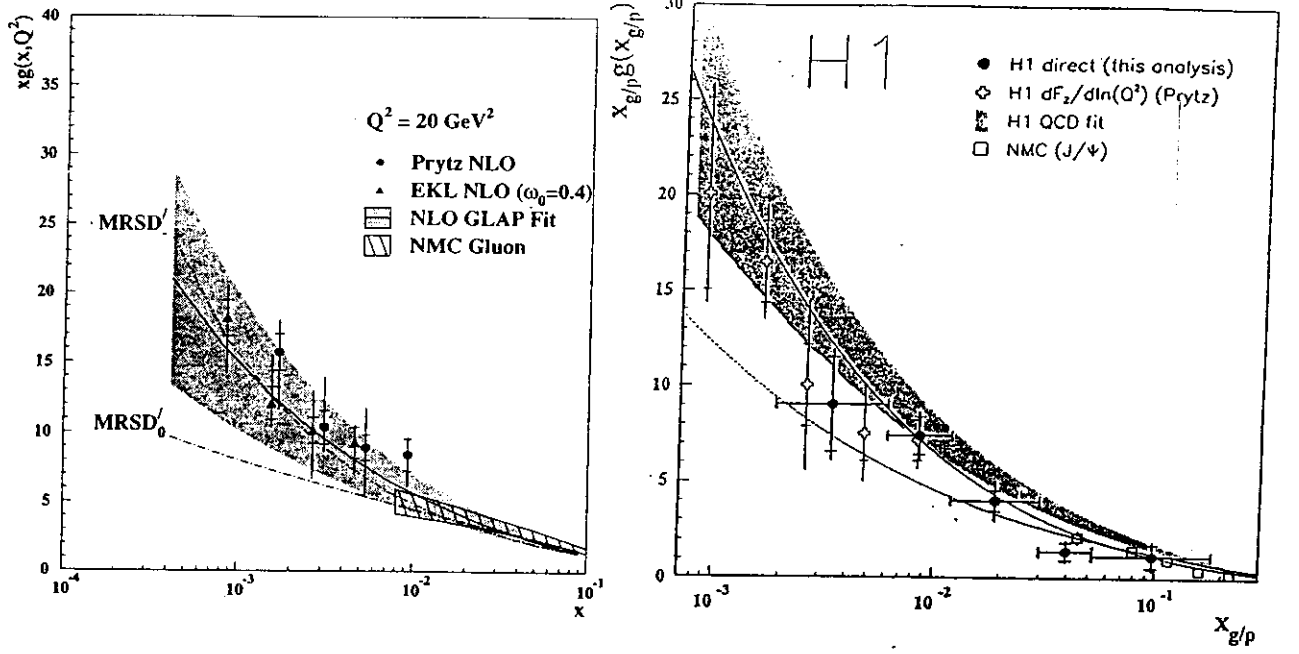
Fig. 4. The gluon momentum density distribution $xg(x, Q^2)$ at a fixed value of Q^2 as determined from the ZEUS data (left) and from H1 data (right). The methods used are explained in the text. In the left figure also the result of a global QCD fit from the NMC data [16] is shown.

to determine $xg(x, Q^2)$ from the scaling violation in F_2 expressed by the GLAP equation for singlet quark distributions:

$$\frac{dF_2(x, Q^2)}{d\ln Q^2} = \frac{\alpha_s(Q^2)}{2\pi}(P_{qq} \bigotimes F2 + P_{qg} \bigotimes \sum_i q_i)$$ (2)

the results of which are shown in Fig. 4:

- Prytz et al. [13] have solved the equation 2 in NLO considering only the second term on the right hand side, which at small x dominates (denoted by 'Prytz NLO').

- Ellis et al. have solved the full equation 2 in the momentum space in NLO assuming a form of $F2$ like: $F_2 = b * x^{\omega_0}$ [14] (denoted by 'EKL NLO'). A fit of this form to the ZEUS data yields $\omega_0 = 0.4$ at $Q^2 = 20\,\mathrm{GeV}^2$.

- A global QCD fit to the F_2 data was performed, using also the NMC data to constrain the fit at large values of x [15].

In a fourth approach the 2+1-jet cross section σ_{2+1} was used to obtain $xg(x, Q^2)$. [2] The cross section σ_{2+1} is related to $xg(x, Q^2)$ by:

$$\sigma_{2+1} = \alpha_s(Q^2)(C_{BGF} \cdot g(x, Q^2) + C_{QCDC} \cdot q(x, Q^2))$$ (3)

where C_{BGF} and C_{QCDC} are the LO QCD coefficient function for the BGF and QCD Compton process. The contribution from QCD Compton events yielding 2+1-jet events has been statistically subtracted

---

[2] the notation 2+1-jet accounts for the fact that the target remnant jet in DIS is counted as an extra jet which is not related to higher order QCD processes

using a Monte Carlo calculation and $xg(x, Q^2)$ was determined using equation 3 and the world average value for α_s [17].

The results for $xg(x, Q^2)$ obtained from all four methods agree within the statistical and systematic errors. A significant increase in the gluon momentum density function with decreasing x is seen in the range $4 \cdot 10^{-4} < x < 10^{-2}$, which is stronger than that observed in the NMC experiment $x > 10^{-2}$. The results show that the scaling violation is dominated by the contribution from the gluon.
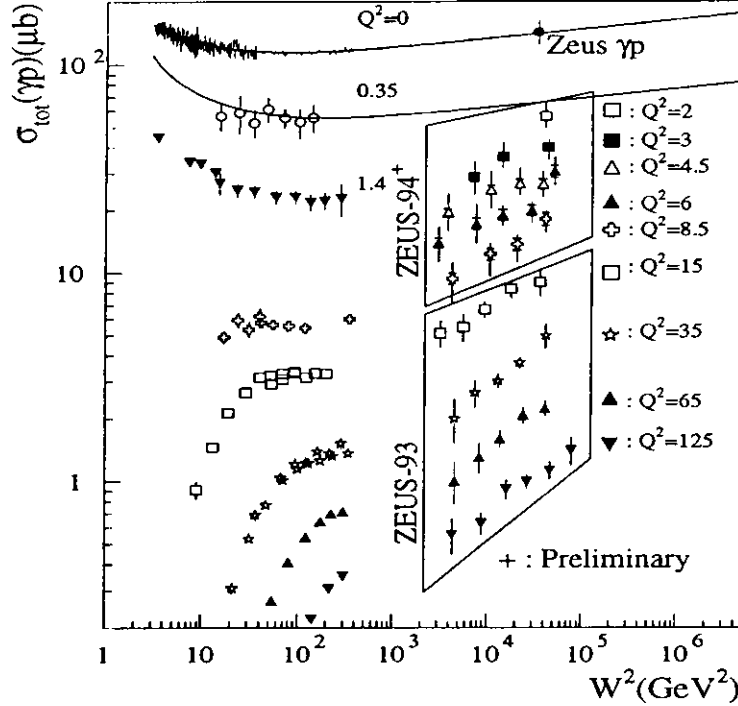
Fig. 5. The total cross section for real photon proton (γp) and virtual photon proton ($\gamma^* p$) interaction at various fixed values of Q^2. The data not marked are from low energy (fixed target) experiments.

At not too high values of Q^2, where the contribution of the Z^0 exchange can be neglected, the DIS cross section can be expressed in terms of the virtual photon flux times the total cross section $\sigma_{tot}^{\gamma^* p}$, which is sum of the cross section σ_L and σ_T for scattering of transverse and longitudinal polarised photons, respectively. The photon flux is well defined if the lifetime of the virtual photon is large compared to the interaction time, i.e. $1/(M_P x) \gg 2R_P$ where M_P and R_P are the mass and the radius of the proton. At small x, $\sigma_{tot}^{\gamma^* p}$ is related to F_2 by:

$$\sigma_{tot}^{\gamma^* p}(x, Q^2) = \sigma_L(x, Q^2) + \sigma_L(x, Q^2) = \frac{4\pi^2 \alpha}{Q^2(1-x)} F_2(x, Q^2) \tag{4}$$

Thus,

$$\sigma_{tot}^{\gamma^* p}(W^2, Q^2) \approx \frac{4\pi^2 \alpha}{Q^2} F_2(W^2, Q^2) \tag{5}$$

where $W \approx \sqrt{Q^2/x}$ for small x is the total γ^*-p c.m. energy. Fig. 5 shows the cross section $\sigma_{tot}^{\gamma^* p}$ as a function of W^2 for fixed values of Q^2 ranging from $Q^2 = 2 \, \text{GeV}^2$ to $Q^2 = 125 \, \text{GeV}^2$. The results for the

6

lower Q^2 bins at high W^2 are based on the recent analysis of data with a shifted vertex position. At high W^2 well above any thresholds, where the above mentioned condition for the photon lifetime is well satisfied, $\sigma^{\gamma^*p}_{tot}$ is rapidly rising with W^2. This is in marked contrast to the total photoproduction cross section $\sigma^{\gamma^*p}_{tot}$ ($Q^2 \approx 0\,\mathrm{GeV}^2$), which exhibits a slow rise, compatible with the W^2 dependence of the total cross section in hadron-hadron interactions and the VDM prediction [18]. One of the most intriguing questions which remains to be answered is, at which value of Q^2 the steep rise of $\sigma^{\gamma^*p}_{tot}$ with W^2 changes to the slow VDM like rise observed for real photons.
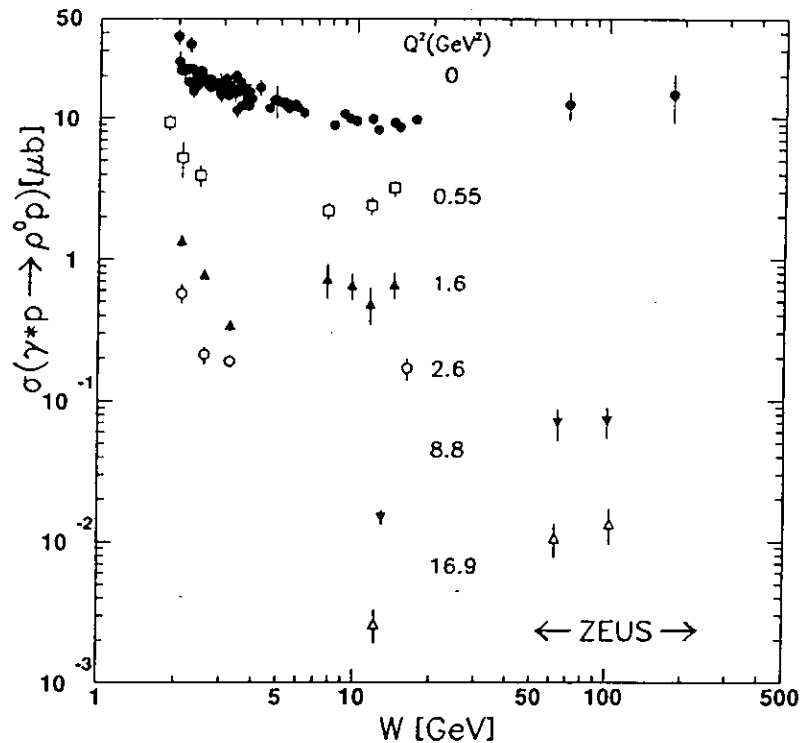
Fig. 6. Compilation of the cross section for elastic ρ^0 production in DIS and photoproduction as a function of W^2 [19].

The total cross section is related to the elastic cross section by the optical theorem. At high W^2 the exchange of the pomeron, which is assigned to diffractive elastic interactions, it dominant compared to the exchange of other Regge trajectories. It is therefore interesting to compare the W^2 dependence of the cross section for elastic ρ^0 production, $\sigma(\gamma^p \to \rho^0 p')$, which is related to the total cross section by the optical theorem, in DIS and photoproduction. A compilation of the data at different values of Q^2 is shown in Fig. 6. As in the case of the total cross section, a significant difference in the slope of the cross section is seen. Again at high Q^2 the W^2 dependence is not compatible with the VDM prediction like for real photons. There are several models which relate the vectormeson production at high Q^2, i.e. at a hard scale, to the gluon density in the proton (e.g. [20, 21]). If this turns out to be right, diffractive processes at high energies may be described in terms of more fundamental processes and the nature of what is called pomeron may become more elucidated.

3 Inclusive Hadron Distributions at High W and Q^2

One of the primary goals of the analysis of the hadronic final state in DIS is the study of QCD effects in the hadronisation. The observation of DIS events with a clear multi-jet structure is the most direct evidence for hard QCD processes. Such events have been studied at high W and Q^2 and have been used to extract the value of α_s and the gluon momentum distribution [22, 23, 17]. With inclusive hadron distributions the studies can be extended also to events, which do not have an unambiguously resolvable jet structure, and the investigation of softer QCD processes. The production of a multi-particle final state in deep inelastic scattering (DIS) is a complicated process which can not be completely calculated in the framework of perturbative QCD. For modelling this process in Monte Carlo programs it is convenient to distinguish two phases of the hadron formation, a perturbative phase for QCD processes on the parton level at high values of Q^2 and a non-pertubative fragmentation phase describing the confinement of the partons in observable hadrons.

The effect of QCD coherence [24] is observed in the Q^2 dependence of the charged hadron multiplicity and of the $\ln 1/x_p$ distribution of charged hadrons in the negative hemisphere of the Breit frame [25, 26], where x_p is the hadron energy in the Breit frame scaled by $Q/2$. More recently the distribution of the scaled longitudinal hadron momentum, x_F, and the transverse hadron momentum, p_t^* in the hadronic centre-of-mass (h.c.m.) frame have been measured. The variable x_F is defined by: $x_F = 2p_{\parallel}^*/W$, with $p_{\parallel}^*$ being the h.c.m. hadron momentum component parallel to the γ^* direction. In fixed target experiments it was found that non-perturbative QCD effects are mingled those of QCD radiation processes on the parton level, which should be calculable in perturbative QCD [27, 28]. The sensitivity to the latter kind of processes is expected to increasse towards large values of W.
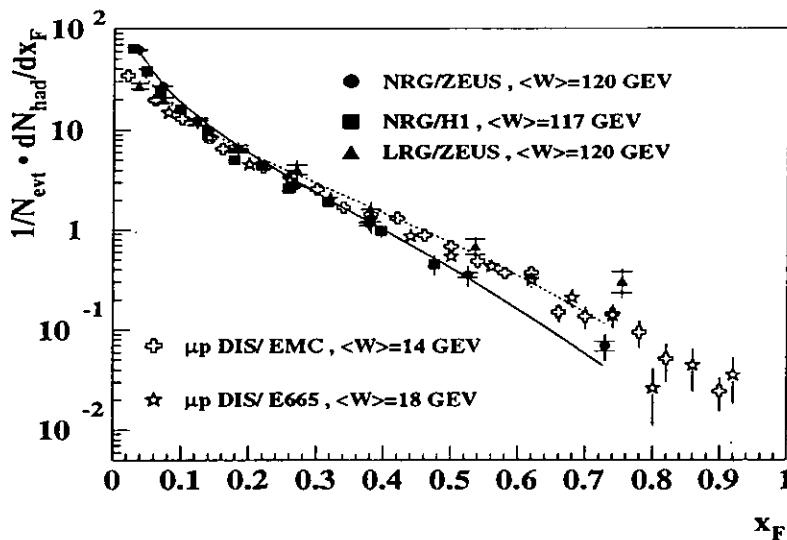
Fig. 7. The x_F distribution for the NRG DIS events measured at HERA by ZEUS [29, 30] and by H1 [31] at $< W >= 120\,\text{GeV}$ compared to the result from a fixed target DIS experiment at $< W >= 14\,\text{GeV}$ [27]. The dotted line shows the prediction of the QPM calculation and the solid line that of the MEPS model calculation. The x_F distribution of the LRG events, which is dicussed in section 4, is also shown here for comparison.

The x_F distributions from various DIS experiments covering a large range of W are shown in Fig. 7. In the data of the HERA experiments the class of events with a large rapidity gap between the observed

8

hadronic final state and the proton direction (LRG events) are excluded and will be discussed separately in section 4. While in the QPM the x_F distribution is predicted to scale in W and Q^2 (dotted line in Fig. 7), a significant violation of the scale invariance in the x_F distribution is observed, which could not be unambiguously identified in the fixed target experiments alone [27, 32]. In order to describe the HERA results,it is necessary to consider QCD radiation processes as it is done in the calculation with the MEPS Monte Carlo program [33] (full line in Fig. 7), where $\mathcal{O}(\alpha_s)$ QCD processes are computed using matrix element formulae (ME) and higher order parton branching processes are simulated in the leading log aprroximation (parton shower PS).

ZEUS 1993
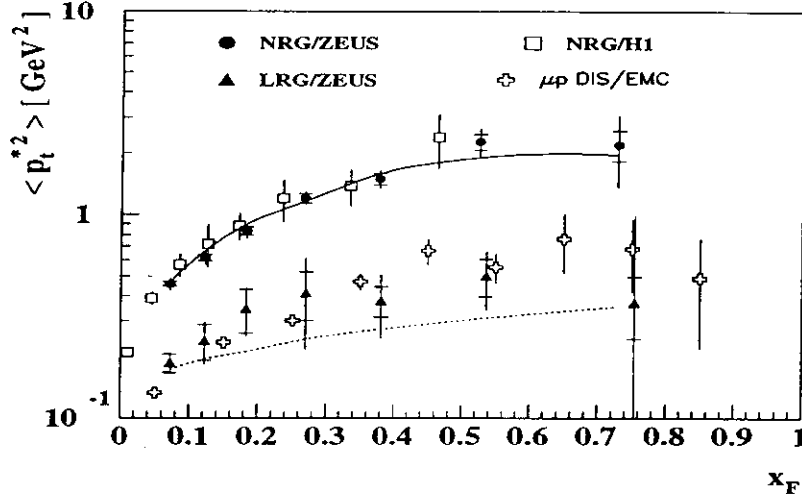
Fig. 8. The mean square of p_t^* for the NRG DIS events measured at HERA by ZEUS [29, 30] and by H1 [31] at $<W> = 120\,\mathrm{GeV}$ compared to the results from a fixed target DIS experiment at $<W> = 14\,\mathrm{GeV}$ [27]. The dotted line shows the prediction of the QPM calculation and the solid line that of the MEPS model calculation. The x_F dependence of $<p_t^{*2}>$ for the LRG events, which is dicussed in section 4, is also shown here for comparison.

The p_t^{*2} distributions have previously been found to be particular sensitive to QCD effects [34]. In Fig. 3 the mean square of p_t^*, $<p_t^{*2}>$, is plotted as a function of x_F. Again the LRG events are excluded from this analysis and discussed later. The result for the non-rapidity-gap (NRG) events is larger by a factor of 2-3 than the values predicted in the QPM (dotted line). The solid line shows the result of a calculation with the MEPS Monte Carlo model [33], which agrees well with the data. At energies reached in the fixed target experiment the values of $<p_t^{*2}>$ [27] are much smaller than those observed at HERA. The comparison with the QPM predition, shows the contribution from non-perturbative QCD processes which are large at low energies (EMC). At HERA energies, however, $<p_t^{*2}>$ is a good observable to test different approaches to calculate the QCD processes on the parton level [29].

4 Large Rapidity Gap Events at High Q^2

In the NC DIS event sample a subclass of events was identified, which is distinguished by a large rapidity gap between the observed hadronic final state and the proton direction. The fraction of these large-rapidity-gap (LRG) events in the total DIS event sample has been found to be independent of Q^2, which shows that the production of LRG events is a leading twist process. The LRG events can be selected

9

by imposing cuts on the variables (η_{max} $\eta_{max} < 1.8$) and $\cos\vartheta_H$ ($\cos\vartheta_H < 0.75$). The pseudorapidity [3] of the particle (cluster in the calorimeter with more than $0.4\,\text{GeV}$ energy deposit) closest to proton direction is denoted by η_{max} and the angle ϑ_H is defined by $\cos\vartheta_H = \sum_i p_{z,i}/|\sum_i p_i|$ (Fig. 9), where p_i is a momentum vector with modulo equal to the energy deposit E_i in a cell i, which points from the ep interaction point to a calorimeter cell i.
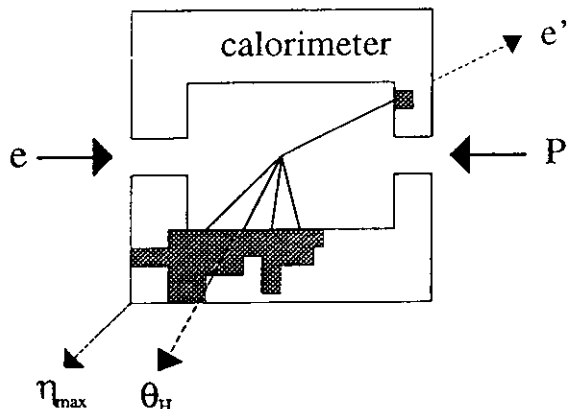
Fig. 9. Schematic figure of an LRG events as seen in the H1/ZEUS detector in order to illustrate the definition of the variables η_{max} and $\cos\vartheta_H$ used to select LRG events.

The distribution of M_X, the invariant mass of the observed hadronic final state, is steeply falling, where as the W and η_{max} distributions are flat. These are properties which are suggestive of diffractive events. The absence of any multi-hadron production in the central and forward rapidity range in the LRG events [35] indicates that there is no colour flux between the direction of the proton and the struck quark.

One possible interpretation of these events is, that there is a colourless particle with which the photon interacts, whereas the proton remains unaffected like in diffractive interactions. This particle could be identified with the pomeron, since diffractive scattering process amongst hadrons have been sucessfully described by the pomeron-exchange picture. One can further assume that the pomeron is short living quantum state with some partonic substructure, which is probed by the virtual photon, such that the photon couples to a pointlike constituent in the pomeron. This would make the leading twist behaviour of the LRG rate plausible. In this picture the variables x_{pom} and β defined in Table 1 have the meaning of being, respectively, the proton momentum fraction carried by the pomeron and the pomeron momentum fraction carried by a pomeron constituent (see Fig. 10). Assuming as a working hypothesis, that the LRG events are events with diffractive dissocation, one can use models for this process, such as the POMPYT Monte Carlo program [36] or the model of Nikolaev and Zakharov [37], to correct the data for acceptance and selection efficiency and to extract the cross section for diffractive DIS. The background of non-diffractive DIS events has to be statisically subtracted using a model for non-diffractive DIS, e.g. the LUND model [33].

The cross section for diffractive DIS can be written in analogy to the non-diffractive DIS cross section in the form:

$$\frac{d^3\sigma}{d\beta dQ^2 dx_{pom}} = \frac{4\pi\alpha^2}{Q^4}\frac{1+(1-y)^2}{2}\cdot F^{D(3)}(\beta, Q^2, x_{pom}) \tag{6}$$

where the cross section has been integrated over $t = (p - p')^2$, since the information from the scattered proton has not been used in this analysis. The function $F^{D(3)}$ is shown in Fig. 11 as a function of

---

[3] the pseudorapidity η is defined by $\eta = -\ln(\tan\frac{\vartheta}{2})$, where ϑ is the polar angle defined with respect to the proton beam direction.

10
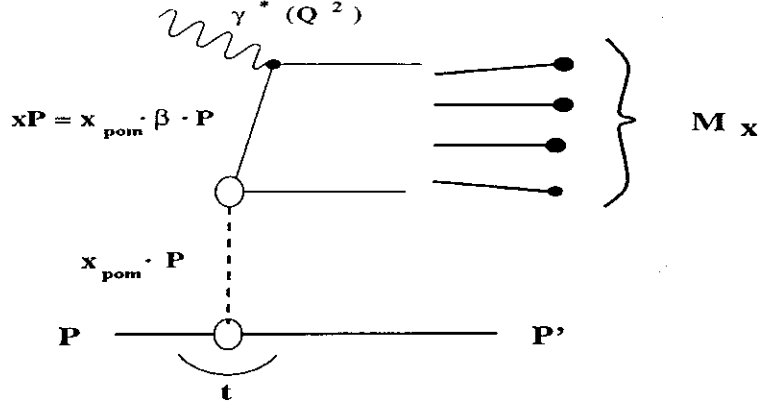
Fig. 10. Schematic diagram of diffractive DIS process. The variables are defined in Table 1.
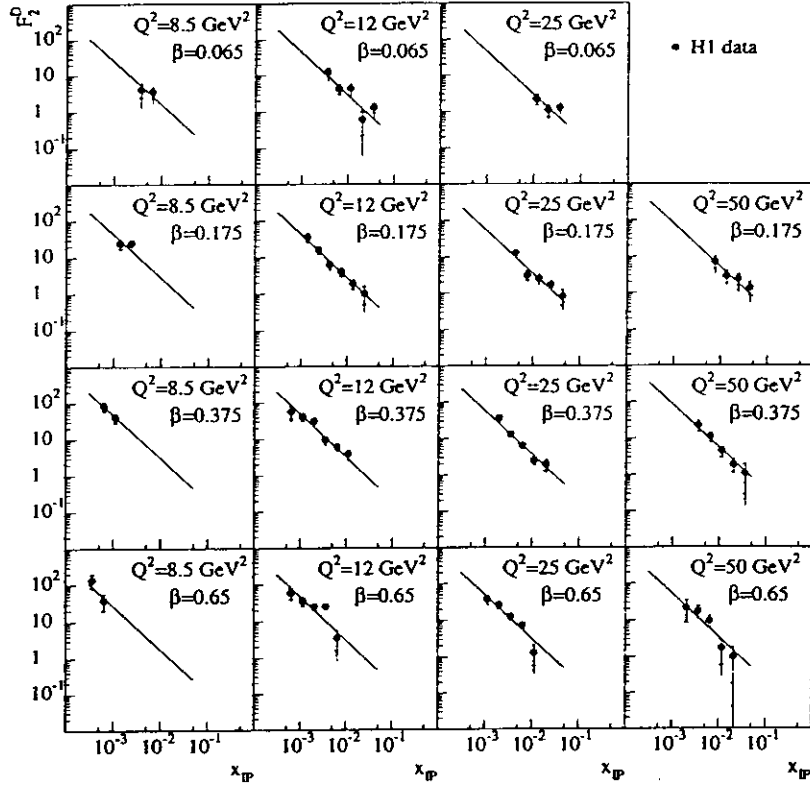
Fig. 11. The function $F^{D(3)}(\beta, Q^2, x_{pom})$ as a function of $x_{I\!P} = x_{pom}$ for different bins of β and Q^2 (from [38]). The inner error bar shows the statistical error, the full error bar the statistical and systematic error added in quadrature. The result of the fit $F^{D(3)}(\beta, Q^2, x_{pom}) = b \cdot (1/x_{pom})^a$ is superimposed.

x_{pom} in bins of Q^2 and β. It can be fitted in all bins of Q^2 and β by the ansatz $F^{D(3)} = b \cdot (1/x_{pom})^a$ with a common parameter a, which was determined to be $a = 1.19 \pm 0.06 \, (stat) \pm 0.07$ (syst) [38] and

11

$a = 1.30 \pm 0.08$ (*stat*) $^{+0.08}_{-0.14}$ (*syst*) [39] by H1 and ZEUS, respectively. The results are consistent with the assumption that the $F^{D(3)}$ can be written in the factorising ansatz as:

$$F^{D(3)}(\beta, Q^2, x_{pom}) = f_{pom/p}(x_{pom}) \cdot F^{D(2)}(\beta, Q^2). \tag{7}$$

In the pomeron exchange picture $f_{pom/p}$ is interpreted as pomeron flux, i.e. the probability to find a pomeron in the proton, and $F^{D(2)}$ as the pomeron structure function. The function $F^{D(2)}$ has been

ZEUS 1993
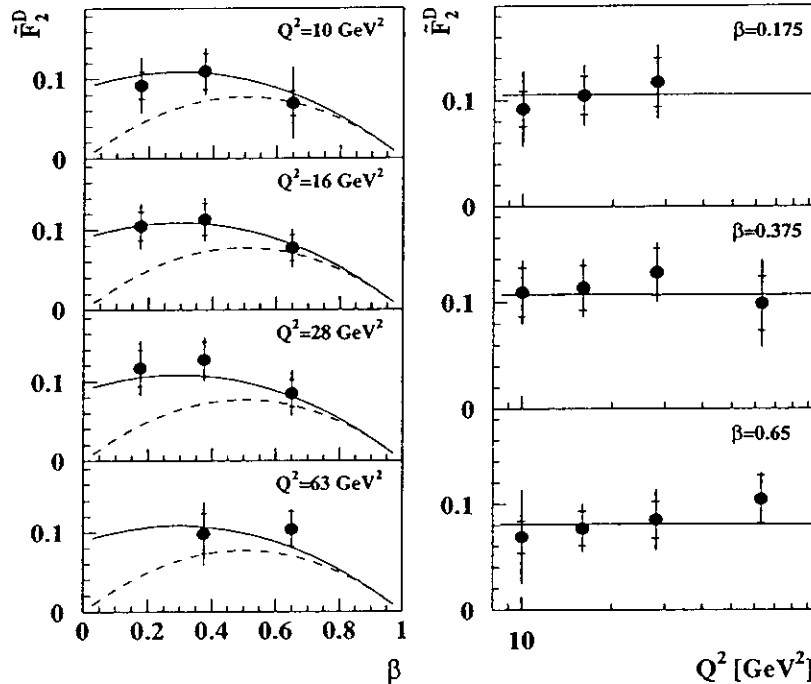
Fig. 12. The function $F^{D(2)(\beta, Q^2)}$ integrated over $6.3 \cdot 10^{-4} < x_{pom} < 10^{-2}$ [39] compared to the parameterisation according to equation 8 (full line) and considering only the $\beta(1 - \beta)$ term (dashed line). The inner error bars show the statistical errors the outer bars show the statistical and systematic errors added in quadrature. The data include an estimated contribution of 15% due to double diffractive dissocation.

obtained by integrating $F^{D(3)}$ over the measured range of x_{pom} using the fitted x_{pom} dependence. The result from the ZEUS experiment [39] is shown in Fig. 12 from the ZEUS data as a function of β in bins of Q^2 and as a function of Q^2 in bins of β; similar results have been obtained from the H1 collaboration [38]. As a function of Q^2 for fixed β the values of $F^{D(2)}(\beta, Q^2)$ are approximately independent of Q^2 for all values of β, which is consistent with a picture where the underlying interaction is the scattering of a virtual photon with point-like quarks within the pomeron. The values of $F^{D(2)}(\beta, Q^2)$ as a function of β for fixed Q^2 are consistent with a flat β dependence as expected from the aligned jet model [40]. The function $F^{D(3)}(\beta, Q^2, x_{pom})$ has been parameterisised in the following form:

$$F^{D(3)}(\beta, Q^2, x_{pom}) = (1/x_{pom})^a \cdot b \cdot \left(\beta(1 - \beta) + \frac{c}{2} \cdot (1 - \beta)^2\right) \tag{8}$$

with $a = 1.3$. The parameterisation assumes factorisation and no Q^2 dependence. It contains a "hard" component of the quark distribution function given by $\beta(1 - \beta)$ term, which has been already favoured

12

by the studies of the inclusive properties of the LRG events [41]. The best fit of the β dependence of $F^{D(2)}(\beta, Q^2)$ using only the quark distribution function shown by the dashed line in Fig. 12 does not agree well with the data at low values of β. By the inclusion of the soft contribution the χ^2 value per degree of freedom of the fit is significantly increased, which indicates that a soft component is required in the pomeron structure function. The power of 2 was adopted from the model of Nikolaev and Zakharov [37].

The approximate factorisation of $F^{D(3)}(\beta, Q^2, x_{pom})$ and the flat β dependence of $F^{D(2)}(\beta, Q^2)$ at fixed Q^2 is also expected in the model of Buchmüller [42], which is not based on the pomeron exchange model. It is demonstrated that the LRG events can be understood as (BGF) process, i.e. a leading twist, non-diffractive DIS process, where the $q\bar{q}$ cluster evolves with a certain probability into a colour singlet parton cluster, which fragments independently from the rest of the nucleon into hadrons. Also in this model $F^{D(3)}(\beta, Q^2, x_{pom})$ can be in a factorising ansatz like in equation 7. However, the terms acquire a different interpretation. The pomeron flux factor $f_{pom/p}$ is replaced by an expression related to the gluon density $g(\xi = x_{pom})$ and the pomeron structure function $F^{D(2)}(\beta, Q^2)$ is identified with differential distribution for the production of a $q\bar{q}$ pair with an invariant mass $M_X = Q^2(1 - \beta)/\beta$. In the pomeron based models the hadrons are produced in the inelastic γ^*-pomeron scattering, whereas in the model of Buchmüller the $q\bar{q}$ pair from the BGF process fragments into hadrons. In both cases the relevant scale of the phase space available for the particle production should be M_X rather than W and the produced hadron spectra should resemble to those of DIS at the appropiate scale of W, namely $W = M_X$. In Fig. 3 values of $<p_t^{*2}>$ as a function of x_F from the LRG event sample [4], are compared to those from NRG events at HERA energies and from an fixed target DIS experiment [27]. The result from the LRG events at $<M_X> = 8$ GeV is in a fair agreement with the that of deep inelastic ep scattering at $<W> = 14$ GeV, whereas the values from the ep scattering at $<W> = 120$ GeV (NRG events) are much larger than those from the LRG events. Also the x_F distribution from LRG events and DIS at $<W> = 14$ GeV agrees within the errors (Fig. 7). The slightly higher values for LRG events at $x_F \gtrsim 0.4$ can be well explained by an effective quark distribution for the LRG events [29], which is harder than the quark distributions in a proton. This confirms, on a qualitative level, the hypothesis arised above.

5   Conclusions

The large increase of the $\gamma^* p$ centre-of-mass energy, W, which can be reached in DIS reaction at HERA has shown a new regime of physics and reveals new phenomena. The rise of F_2 towards small x at fixed Q^2 signals a rapid increase of the parton densities, which can be explained by gluon radiation as described by the GLAP evolution equations. The rise of F_2 is equivalent to a increase of $\sigma_{tot}^{\gamma^* p}$ with rising W^2 which is in contrast to the W^2 dependence of $\sigma_{tot}^{\gamma^* p}$. The same qualitative difference in the W^2 dependence is also seen for the cross section for elastic ρ^0 production with virtual and real photons. The extension of the measurements of $\sigma_{tot}^{\gamma^* p}$ to values of Q^2 of the order of 0.3 GeV^2 is most interesting to study the transition between the real and virtual photon interaction with the proton.

The other very compelling observation in DIS events at HERA is the observation of large rapidity gap events at high Q^2. The mechanism for producing this kind of events is still not known. Roughly speaking, there are two alternative approaches: the one is based on the pomeron exchange picture which was successfully applied in diffractive hadron-hadron interactions. And the other interpretes the LRG events as BGF, i.e. non-diffractive DIS events, with soft colour exchange which is reponsible for the decoupling of the fragmentation of the $q\bar{q}$ system from the target remnant. In both cases the cross section can be factorised as described in equation 7. With the present data it is not yet possible to measure the β and Q^2 dependence with sufficient accuracy to distinguish between the different models.

---

[4]This LRG sample was selected by requiring $\eta_{max} < 1.5$ so that the background from non-diffractive DIS is $< 5\%$ in the kinematic region considered.

However, not only a higher accuracy of the DIS cross section measurements is necessary, but also the comparison of the results for DIS at low x with those of other high energy reactions and a more detailed analysis of the structure of the LRG events. Considering the non-pomeron based model, the BGF events exhibit a large rapidity gap, if the $q\bar{q}$ system fragments independently and the proton does not lose so much momentum, that it breaks up and produces a multi-hadron final state with a high invariant mass. This would imply that the fraction of LRG events should decrease towards large x at fixed W. It also would be important to test, whether the probability of a colour exchange, which is assumed to change the $q\bar{q}$ system from a colour octet to a colour singlet state, changes for DIS on nuclei. In order to test the pomeron bases models, it is essential to compare the inclusive properties and the hadron distributions of LRG events with those of diffractive hadron-hadron or photoproduction processes.

The investigation of NRG and LRG events have yielded exciting results and it can be expected that the future experimental results test the proton structure and the dynamics of strongly interacting objects at a very fine scale and considerably improve the understanding of other high energy reactions.

References

[1] M. Virchaux, Proc. of Int. Workshop 'QCD - 20 Years Later', Aachen (1992), p 205.

[2] T. Sloan, G. Smadja, R. voss, Phys. Rep. 162 (1988) 45.

[3] N. Schmitz, Int. J. Mod. Phys. A8 (1993) 2026.

[4] H1 Collab., I. Abt et al., Nucl. Phys. B407 (1993) 515.

[5] ZEUS Collab., M. Derrick et al., Phys. Lett. B316 (1993) 412.

[6] ZEUS Collab., M. Derrick et al., Z. Phys. C65 (1995) 379.

[7] H1 Collab., I. Ahmed et al., Nucl. Phys. B439 (1995) 471.

[8] NMC Collab., P. Amaudruz et al., Phys. Lett. B259 (1992) 159.

[9] M. Glück, E. Reya, A. Vogt, Phys. Lett. B306 (1993) 391;
    M. Glück, E. Reya, M. Stratmann, Univ. Dortmund DO-TH 93/20 (1993).

[10] A.D. Martin, R.G. Roberts, W.J. Stirling, Phys. Lett. B306 (1993) 145.

[11] V.N. Gribov, L.N. Lipatov, Sov. Journ. Nucl. Phys. 15 (1972) 438 and 675;
     G. Altarelli, G. Parisi, Nucl. Phys. B126 (1977) 297;
     Y.L. Dokshitzer, Sov. Phys. JETP 46 (1975) 641.

[12] L.N. Lipatov, Sov. J. Nucl. Phys. 23 (1976) 338;
     E.A. Kuraev, L.N. Lipatov, V.S. Fadin, Sov. Phys. JETP 45 (1977) 199;
     Y.Y. Balitskii, L.N. Lipatov, Sov. J. Nucl. Phys. 28 (1978) 822.

[13] K. Prytz, Phys. Lett. B332 (1994) 393;
     K. Prytz, Phys. Lett. B311 (1993) 286.

[14] R.K. Ellis, Z. Kunszt, E.M. Levin, Nucl. Phys, B420 (1994) 517.

[15] ZEUS Collab., M. Derrick et al., Phys. Lett. B345 (1995) 576.

[16] NMC Collab., M. Arneodo et al., Phys. Lett. B309 (1993) 222.

[17] H1 Collab., I.Ahmed et al., DESY 95-86 (1995), subm. to Nucl. Phys. B..

[18] A. Donnachie, P.V. Landshoff, Nucl. Phys. B244 (1984) 322;
A. Donnachie, P.V. Landshoff, Nucl. Phys. B267 (1985) 690.

[19] ZEUS Collab., M. Derrick et al., DESY 95-133 (1995), subm. to Phys. Lett. B.

[20] S.J. Brosdky et al., Phys. Rev. D50 (1994) 3134.

[21] M.G. Ryskin, Z. Phys. C57 (1994) 89.

[22] H1 Collab., I.Abt et al., Z. Phys. C 61 (1994) 59;
H1 Collab., I.Ahmed et al., Phys. Lett. B346 (1995) 415.

[23] ZEUS Collab., M. Derrick et al., Z. Phys. C67 (1995) 81.

[24] Yu. Dokshitzer, V. Khoze, A. Mueller and S. Troyan, "Basics of Perturbative QCD", Editions Frontières, Gif-sur-Yvette, France (1991).

[25] ZEUS Collab., M. Derrick et al., Z. Phys. C67 (1995) 93.

[26] H1 Collab., I. Abt et al., DESY 95-072 (1995), submitted to Nucl. Phys. B.

[27] EMC Collab., J. Ashman et al., Z. Phys. C52 (1991) 361.

[28] EMC Collab., M. Arneodo et al., Z. Phys. C36 (1986) 527;
EMC Collab., M. Arneodo et al., Z. Phys. C35 (1986) 417.

[29] N.A. Pavel, Habilitationsschrift (University Hamburg Oct.'94), DESY 95-147 (1995).

[30] N.A. Pavel, Proceedings of the QCD Workshop, Paris, April 1995 (in prep.)

[31] H1 Collab., I. Abt et al., Z. Phys. C63 (1994) 377.

[32] E665 Collab., M.R. Adams et al., Phys. Rev. D50, 1836 (1994).

[33] G. Ingelman, Proc. of the Workshop on 'Physics at HERA', DESY (1992) 1366.

[34] EMC Collab., J.J. Aubert et al., Phys. Lett. B95 (1980) 306.

[35] ZEUS Collab., M. Derrick et al., Phys. Lett. B338 (1994) 483.

[36] P. Bruni, G. Ingelman, DESY 93-187.

[37] N.N. Nikolaev, B.G. Zakharov, Z. Phys. C53 (1992) 331.

[38] H1 Collab., I. Ahmed et al., Phys. Lett. B348 (1995) 682.

[39] ZEUS Collab., M. Derrick et al., DESY 95-115 (1995).

[40] J.D. Bjorken, J. Kogut, Phys. Rev. D8 (1973) 1341.

[41] ZEUS Collab., M. Derrick et al., Phys. Lett. B315 (1993) 481.

[42] W. Buchmüller, Phys. Lett. B335 (1994) 479;
W. Buchmüller, DESY 95-065 (1995); W. Buchmüller,A. Hebecker DESY 95-077 (1995).